On the numerical analysis of the Fabry-Pérot interferograms*

ANDRZEJ BIELSKI, WACŁAW DOKURNO, JAN WASILEWSKI, JERZY WOLNIKOWSKI

Institute of Physics, Nicholas Copernicus University, Toruń, Poland.

Three methods of numerical determination of the Voigt profile parameters from Fabry–Pérot (FP) interferogram have been discussed and tested. The error simulation has been performed assuming that the error comes from the finite number of photons in the signal. The influence of the dark current of the photo-multiplier as well as the slow changes of the intensity of light source during the registration time have also been studied. The smallest value of the light intensity at the maximum of the line and the region of the Lorentzian and Gaussian widths, at which the realiable data may be obtained, have been estimated.

Introduction

This paper deals with the analysis of profiles of pressure-broadened spectral lines performed by means of Fabry–Pérot interferometers. In many cases experimental data on line broadening in the very low pressure region reported by various researchers differ markedly, in particular for weak lines. As an example the "laser" line of neon $\lambda = 632.82$ nm may be quoted. For this line MATYUGIN et al. [1] found two different values of the pressure broadening coefficient $a = d(\varDelta v_L)/dp$ ($\varDelta v_L$ — Lorentzian width of the line, p — pressure), namely $(2.1 \pm 0.14) \times 10^{-5}$ cm^{-1} Pa and $(1.5 \pm 0.1) \times 10^{-5}$ cm^{-1} Pa, using two methods of data analysis. Similar situation was reported by MATYUGIN et al. [1] for the $\lambda = 543.37$ nm line of neon. For a strong line $\lambda = 585.2$ nm, however, the same authors have obtained the identical value of a by using different methods of profile analysis. Very large discrepancies exist for the NeI line $\lambda = 582.02$ nm, where two different methods of data analysis yielded the values $a = 7.5 \times 10^{-5}$ cm^{-1} Pa [2] and 1.8×10^{-5} cm^{-1} Pa [3].

These discrepancies are probably due to the accuracy of the numerical procedure applied to the analysis of line profiles and to the different propagation of experimental errors in different methods.

Three different procedures of determining the Lorentzian and Gaussian widths of spectral line are here discussed. In particular a procedure, which consists of direct comparison of the measured line shape with the Voigt profile, with the inclusion of overlaping of interference orders is discussed. The accuracy of this procedure as well as of two other

---

procedures for determining the Lorentzian and Gaussian width has been tested.

In the present work a particular attention has been paid to the error propagation in these methods. To this aim the method of error simulation was used which also enabled to estimate the lowest values of the signal at the maximum of line at which reliable results could still be obtained.

Numerical analysis of the Fabry-Pérot interferograms

The detection of signal in a spectrometer with the Fabry–Pérot inter-ferometer (FPI) can be performed either by a direct data recording by a recorder, or by digital methods using a scalar or a multichannel analyser. In the case of the digital detection of signal the results are obtained in the form of a sequence of positive integers. An example of an interfero-gram obtained from the FPI by means of a digital method is shown in fig. 1. This interferogram was obtained for the $\lambda = 568.93$ nm line of
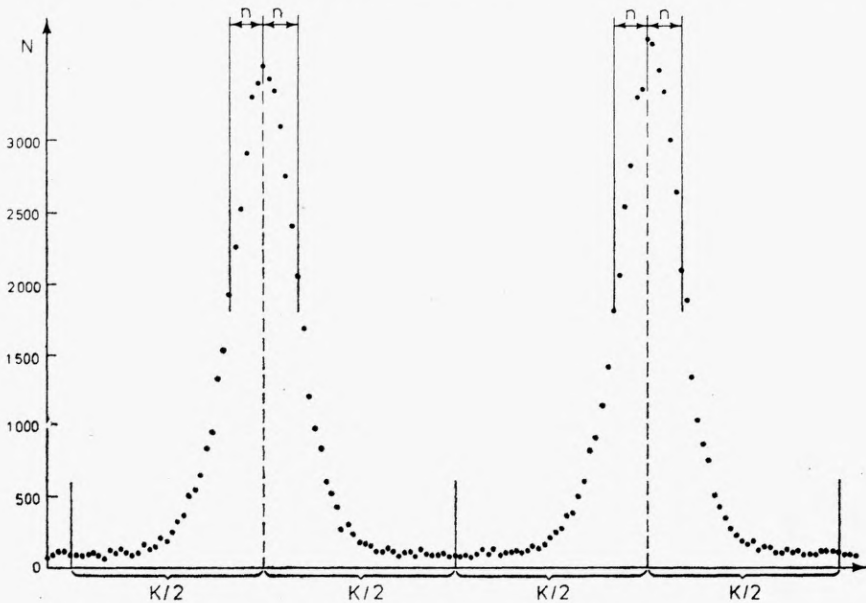
Fig. 1. The interferogram of the *NeI* $\lambda = 568.9$ nm spectral line. N — the number of counts (for explanation see text)

neon by means of the spectrometer described recently [4] using a glow discharge tube at neon pressure 1.06×10^{-2} Pa and the discharge current 1.45 mA, with the spacer 1.513 cm.

Our computer analysis of the interferogram begins with searching for the abscissa of maximum for each interference order. For this purpose two algorithms have been programmed. The first one is based on the assumption that the line profile is symmetric in the vicinity of its maxi-

mum. This assumption is justified for the low-pressure experiments. The program finds n points (n being an input value) on both the side of the highest point of the whole profile (cf. fig. 1). Having determined the set of these $2n+1$ points, the program uses every subset of $3, 4, \ldots, 2n+1$ points (not all of them laying on the same side of maximum) to determine the parabola by means of the least square fit. The arithmetic mean of all the abscissae of these parabolae maxima is taken as the abscissa of the maximum, excluding the parabolae having no maxima within the accepted range of $2n+1$ points (the latter concerning the cases where the parabola has either a maximum outside this range, or a minimum due to noise).

The second algorithm can be used for the analysis of asymmetric profiles. In this case, after determining of the set of $2n+1$ points as described above, every subset of $2, 3, \ldots, n$ points (all lying on the same side of the profile) is used to determine the straight line by means of the least squares fit. Then the intersection points of every pair of these lines are found, the left-side line and the right side one having positive and negative derivatives, respectively. The arithmetic mean of all the crossing point abscissae is accepted as the abscissa of the maximum analysed. This "linear" algorithm is, however, not further discussed, because the profiles analysed in this paper are rather symmetric and the first (parabolic) algorithm appeared to be successful. The possibility of combining both the algorithms is also programmed.

To determine the maximum for the next interference order the program searches for the highest points of the whole profile, excluding of the $2n+1$ points already analysed. The maximum is then found by using the same algorithm as for the first maximum. This process is continued until the given number of the interference orders is analysed. Next, the program finds the average distance K between the maxima. The range of $\pm K/2$ (from the left to the right side of every maximum, cf. fig. 1) is now identified with the dispersion range from $-1/4t$ to $+1/4t$ (t — the distance between the interferometer plates) and the abscissa of every point within the given interference order is expressed in the units of $1/2t$. Then the profiles of all the interference orders are shifted and overlayed with each other in such a way, that the abscissae of all the maxima previously calculated fall into the same point. In this way the program produces the "composed" profile, in which the points lying outside the interval $\pm 1/4t$ are omitted. Fig. 2 presents the "composed" profile obtained from the interferogram shown in fig. 1. Basing on this "composed" profile the function values in the equidistant points are calculated using the parabolic interpolation.

The experimentally observed line profile $B(\tilde{\nu})$ is a convolution of the Fabry–Pérot instrumental function $A(\tilde{\nu})$ and the "true" line profile $I(\tilde{\nu})$:
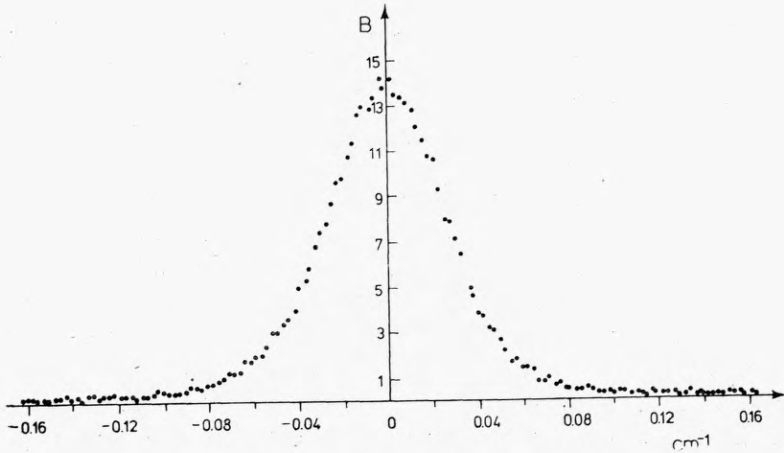
Fig. 2. The observed shape of the *NeI* $\lambda = 568.9$ nm line obtained from the interferogram shown in fig. 1

$$B(\tilde{\nu}) = \int\limits_{-\infty}^{\infty} A(\tilde{\nu}-\tilde{\nu}')I(\tilde{\nu}')d\tilde{\nu}' \tag{1}$$

where $\tilde{\nu}$ — wavenumber.

Formally, the profile $I(\tilde{\nu})$ can be found by using the Fourier transform method. Let $a(s)$ and $b(s)$ denote the Fourier transforms of the $A(\tilde{\nu})$, $B(\tilde{\nu})$ functions, respectively. Then $I(\tilde{\nu})$ is given by

$$I(\tilde{\nu}) = \frac{1}{2\pi} \int\limits_{-\infty}^{+\infty} \frac{b(s)}{a(s)} e^{-2\pi i\tilde{\nu}cs} ds \tag{2}$$

(the integration variables s has the meaning of time). If the transform $a(s)$ becomes zero for some values of s, the unique solution of (2) is not possible. Moreover, if there are no a priori assumptions concerning the properties of the $I(\tilde{\nu})$ function, the experimental errors may cause a rather big uncertainty of the solution. This uncertainty can be avoided, however, under some assumptions on the spectral line shape, cf. [5]. In our analysis we have assumed, that $I(\tilde{\nu})$ is the Voigt profile.

$$I(\tilde{\nu}) = I_0 \int\limits_{-\infty}^{\infty} \frac{\exp[-(2\sqrt{\ln 2}\, y/\Delta\tilde{\nu}_D)^2]}{(\Delta\tilde{\nu}_L/2)^2+(y-\tilde{\nu})^2} dy; \tag{3}$$

where I_0 — normalizing factor; $\Delta\tilde{\nu}_D$, $\Delta\tilde{\nu}_L$ — Doppler and Lorentzian half-width, respectively, and the integration variable y has the meaning of the wavenumber.

Here we investigate three methods of the line shape analysis, using the additional assumption that the Fabry–Pérot instrumental function $A(\tilde{\nu})$ can be represented by the Airy function:

$$A(\tilde{\nu}) = \frac{A_0}{1 + F \sin^2\left[\dfrac{\pi}{\Delta\tilde{\nu}_i}(\tilde{\nu} - \tilde{\nu}_0)\right]}, \tag{4}$$

where:

$F = 4R/(1-R)^2$,

R — reflectance of the interferometer plates,

$\tilde{\nu}_0$ — wavenumber of the line maximum,

$\Delta\tilde{\nu}_i$ — the free spectral range of the interferometer,

A_0 — normalization factor.

Method 1

According to BALLIK [6] the convolution of the FPI-Airy function and the Voigt profile can be expressed analytically as follows:

$$G(x) = \frac{B(x)}{B(0)} = \frac{\frac{1}{2} + \sum\limits_{n=1}^{\infty} (\mathrm{Re}^{-L})^n e^{-n^2 D^2/4} \cos(nx)}{\frac{1}{2} + \sum\limits_{n=1}^{\infty} (\mathrm{Re}^{-L})^n e^{-n^2 D^2/4}}, \tag{5}$$

where:

$$L = \pi\Gamma_L, \tag{6}$$

$$D = \frac{\pi}{\sqrt{\ln 2}}\,\Gamma_D, \tag{7}$$

$$x = 2\pi(\tilde{\nu} - \tilde{\nu}_0)/\Delta\tilde{\nu}_i \tag{8}$$

$$\Gamma_L = \Delta\tilde{\nu}_L/\Delta\tilde{\nu}_i, \quad \Gamma_D = \Delta\tilde{\nu}_L/\Delta\tilde{\nu}_i. \tag{8a}$$

Let Δx denote the half-width of the function $G(x)$. In the Ballik method the ratio $B(\pi)/B(0)$ and the ratio of the half-width Δx to the free spectral range $\Delta\tilde{\nu}_i$ should be determined. Next, the values of D and Re^{-L} can be found graphically. In order to calculate the $B(\pi)$ and $B(0)$ values, the parabolic interpolations are used within the range of 0.12 and 0.07 of interference order, respectively. The half-width Δx is then found from $B(0)$ using the linear interpolation within the range of 0.04 of the interference order. The numerical values quoted above were determined by tentative calculations (numerical experiment). These values correspond to the cases for which the ratio $\Delta x/2\pi$ ranges from about 0.1 to about 0.35.

Method 2

In this method the experimentally observed periodic function $B(x)$ is reduced to an aperiodic function $B_1(x)$ in the interval $[-\pi, \pi]$:

$$B_1(x) = B(x) - r(x), \tag{9}$$

where $r(x)$ represents the contribution due to the higher interference orders. If the Fabry–Pérot instrumental function is the Airy function, it can be expanded into the series of the Lorentz profiles (cf. e.g. [7])

$$A(x) = A_1 \sum_{n=-\infty}^{\infty} \frac{1}{1 + 4\left(\dfrac{x + n\pi}{M}\right)^2}, \tag{10}$$

where:

$$M = -\frac{\Delta\tilde{\nu}_i}{\pi} \ln R, \tag{11}$$

A_1 — normalization factor,
x — is given by (8).

If the true line profile is of the Voigt type, (eq. (3)), then $B_1(x)$ is also the Voigt profile, with the Lorentzian component

$$\Delta\tilde{\nu}'_L = \Delta\tilde{\nu}_L - \frac{\Delta\tilde{\nu}_i}{\pi} \ln R. \tag{12}$$

In the first approximation, valid when the half-width of $B(x)$ is small, compared to $\Delta\tilde{\nu}_i$, the $r(x)$ function in the interval $[-\pi, \pi]$ can be expressed as:

$$r(x) \approx B(\pi)\left[\frac{1}{\sin^2\left(\dfrac{x}{2}\right)} - \frac{1}{\left(\dfrac{x}{2}\right)^2}\right]$$

$$= B(\pi)\left[\frac{1}{3} + \frac{1}{15}\left(\frac{x}{2}\right)^2 + \frac{2}{189}\left(\frac{x}{2}\right)^4 + \dots\right]. \tag{13}$$

Using the new variable

$$h = \frac{\Delta\tilde{\nu}_D}{\Delta\tilde{\nu}'_L + \Delta\tilde{\nu}_D} \tag{14}$$

we tabulate the function

$$\varepsilon(h) = \Delta x_1 \cdot B_1(0) \left[\int_{-\infty}^{\infty} B_1(x)\,dx\right]^{-1}, \tag{15}$$

where Δx_1 — the half-width of the $B_1(x)$ function. We also tabulate the function

$$Y(h) = \frac{\Delta x_1}{\Delta \tilde{\nu}'_L + \Delta \tilde{\nu}_D}. \tag{16}$$

From (10) it follows that

$$\int_{-\pi}^{\pi} B(x)\,dx = \int_{-\infty}^{\infty} B_1(x)\,dx.$$

In practical calculations the function $B(x)$ is normalized to unity within one interference order:

$$\int_{-\pi}^{\pi} B(x)\,dx = 1. \tag{17}$$

The values of $B_1(0)$ and Δx_1 can be found in the same way as in the method 1. Then, the value of h can be found from the table of $\varepsilon(h)$ function, and the value of Y from the table of $Y(h)$. Finally, the half-widths $\Delta \tilde{\nu}'_L$ and $\Delta \tilde{\nu}_D$ can be found from eqs. (14) and (16). The tables of functions $\varepsilon(h)$ and $Y(h)$ are presented in the Appendix.

Method 3

The values of half-widths $\Delta \tilde{\nu}'_L$ and $\Delta \tilde{\nu}_D$, obtained by the method 2, are used in the formula (5) to determine L and D, under the additional normalization condition (17). The iterative algorithm based on the least squares fit is used.

These three methods have been programmed in the Algol-1204 autocode for the Odra 1204 computer. The program needs the segmentation and uses the drum storage. It is available on request. For a rather typical case of the interefrogram having two interference orders ($\sim$140 experimental points) the maxima being determined by means of the parabolic algorithm, with $n = 6$, the total computation time is $\sim$15 min.

Tests and simulation

All the three methods of the analysis of interferograms discussed above are developed for the case of an isolated spectral line. They can be, however, applied also in case of lines having non-entirely resolved structures. In such a case the shape of total line should be reduced numerically to that of the isolated line. In the present work we consider the case of two ovarlapping lines so that the line shape $H(x)$ my be represented as the sum:

$$H(x) = c[G(x) + \beta G(x + \delta)], \tag{18}$$

where c is the number of pulses at the maximum of the line at any count-
ing time, β — the relative intensity of the second component, δ — the
distance between components, $G(x)$ is the shape of the isolated line.

If the distribution $H(x)$ is known the distribution $G(x)$ can be found
by using the method described in [8]. This method, being an identity
transformation, does not introduce any additional errors. In this method
one assumes that both the components have identical shapes and the
parameters β and δ are known. The distribution $G(x)$ determined in this
way has been further analysed using the three methods discussed above.
Here (and in the further text) we use the term "Lorentzian width" for
the sum of the real Lorentzian width $\Delta\tilde{\nu}_L$ and the instrumental width,
i.e. for

$$\Delta\tilde{\nu}_L = \frac{\Delta\tilde{\nu}_i}{\pi}\ln R. \tag{19}$$

For given values of parameters describing the distribution $G(x)$,
i.e., $\Delta\tilde{\nu}_L$ and $\Delta\tilde{\nu}_D$, the function $H(x)$ was tabulated at 68 points within
one interference order, i.e. the period of function was divided into 68
parts. Two periods of the function were taken into account in the com-
putations. In our calculation we assumed that $\beta = 0.1$, $\delta = 0.2\pi$.

The first step in our test was to study the accuracy of the methods
under consideration. Therefore a series of calculations have been per-
formed for the accurate values of the function $H(x)$, and various values
of Γ_L and Γ_D. The relative errors of the calculated Γ_L and Γ_D values,
resulting from: the procedure of the "composed" curve construction
(described above), elimination of the second component and the numerical
analysis of the interferogram, appeared to be below 0.2%.

In view of the fact that the results of the digital detection are obtained
in the form of sequence of positive integers, the values of $H(x)$ have
been approximated by the nearest integers.

The normalizing factor c in eq. (18) simulates the number of the
counted pulses at the maximum of the line and in the time interval,
within which the counting is carried out. By performing the calculation
for various values of c we can estimate the lower limit of the signal at the
line maximum, at which these methods give realiable results. Such cal-
culations were performed for five values of c ($c = 200$, 500, 1000, 2000,
and 4000) and for 4 values of Γ_L (0.015, 0.03, 0.06, and 0.12). In all the
calculations the same value of $\Gamma_D = 0.18$ has been used. The analysis
of the results obtained showed that if the number of pulses at the ma-
ximum is below 500 than the accuracy of all the methods drastically
decreases due to the approximation of $H(x)$ by the nearest integer. For
small c this approximation yields a curve similar to the step curve, which
is constant within large intervals in the vicinity of minimum. Therefore,
in all further calculations we have assumed that $c > 500$. In order to

test an error propagation in the considered methods we have performed a simulation of both the error for the function describing the observed line shape and the background of the photomultiplier. Then using a generator of random numbers we generate a sequence of numbers from the interval $(0, 1)$. The first number of this sequence is interpreted as the value of the distribution function of the standard normal distribution $N(0, 1)$ (cf. [9]). Further using the Kahn approximation for the distribution $N(0, 1)$, the distribution function $\Phi(u)$ has been expressed as (for the positive half-axis, cf. [10]):

$$\Phi(u) = \frac{1}{\sqrt{2\pi}}\, e^{-u^2/2} \approx \frac{k e^{-ku}}{(1+e^{-ku})^2}, \; u > 0, \tag{20}$$

where $k = \sqrt{8/\pi}$. We can find the value of v:

$$v = 2 \int_0^u \Phi(u)\, du, \; u > 0.$$

We can also find the normalized variable u [10]:

$$u = \frac{1}{k} \ln \frac{1+v}{1-v}; \; 0 < v < 1. \tag{21}$$

The normalized variable u, found in this way, is defined for the positive half-axis. In order to get its value for all the real numbers we study the next number from the series of the random numbers. If it is smaller than 0.5 we take $-u$ as the final value of the normalized variable, and if it is greater than or equal to 0.5 we take $+u$. In this way for each pair of random numbers generated in the interval $(0, 1)$ we obtain one value of the normalized variable u. Since the counting of pulses is described by the Poisson distribution, we assume that the mean standard deviation is $\sqrt{H(x)}$, while the values of $H(x)$ are given by eq. (18) and $H(x) + u\sqrt{H(x)}$ was taken as the final value of the "signal" at the given measured point. Usually during the measurements various phenomena, such as desorption of gases, may appear inside the light source (e.g. discharge tube). These effects may cause a decrease of the signal in a way very similar to the decrease due to the phenomena of quenching in atomic and molecular systems. Therefore, those effects will be called "quasi-quenching".

In order to include such "quasi-quenching" into our analysis we have assumed that the decrease of the signal within one interference order may be described by a formula:

$$I(x) = \frac{I_0(x)}{1 + qx}, \tag{22}$$

where $I_0(x)$ denotes the value of signal at the abscissa x when there is no "quasi-quenching" and q is a constant parameter. This form of $I(x)$

was assumed in analogy to the well-known Stern–Volmer formula describing the real quenching [11]. In our calculation the parameter q was determined by assuming that the decrease of the signal between the first point of the interferogram and the point situated at the distance equal to one interference order is equal to 10%. The comparison of the results of calculations, with inclusion and omitting of the "quasi-quenching", has proved that the decrease of the signal smaller than 10% does not introduce any essential errors. It turned out that the error of calculated values Γ_L and Γ_D caused by the "simulated error" is much greater than the error due to the decrease of the intensity of the source caused by "quasi-quenching".

The first step in the analysis of interferograms is to determine the positions of particular maxima and their distances from one another. The accuracy of the "composing procedure", which gives the "composed" profile, has the most essential influence on the errors of all the methods.

Results of calculations of the position of the first interferogram maximum, for which the decrease of signal due to "quasi-quenching" is the largest one, are presented in fig. 3 as a function of the value c of the signal at the maximum.

Figure 4 shows the distance between the neighbouring maxima, determined from six different distributions of errors on the curve, as a function
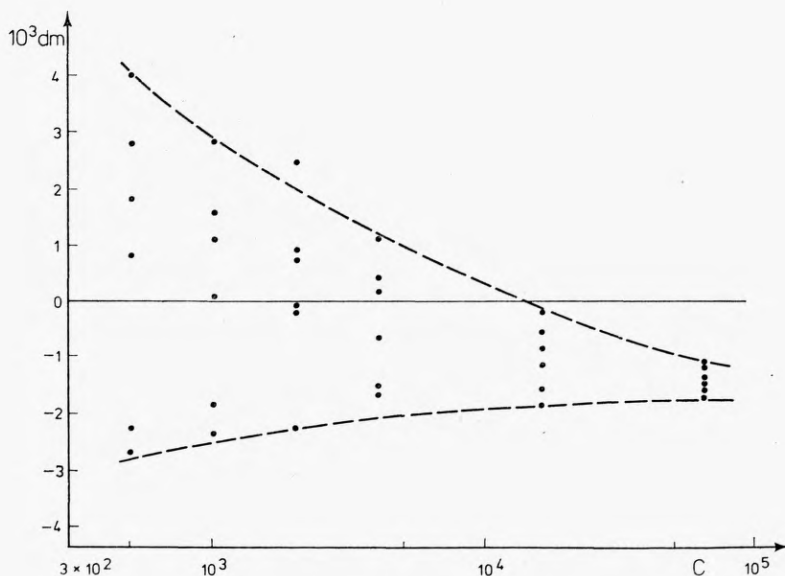
Fig. 3. The deviation dm of the determined position, of the first interference maximum as a function of the value c of the signal at the maximum (for $\Gamma_L = 0.03$, $\Gamma_D = 0.18$). The assumed accurate position of the maximum is for $dm = 0$. The deviation dm is given in parts of the distance between the maxima. The points show the values dm for various distributions of errors on the curve for a given value of c
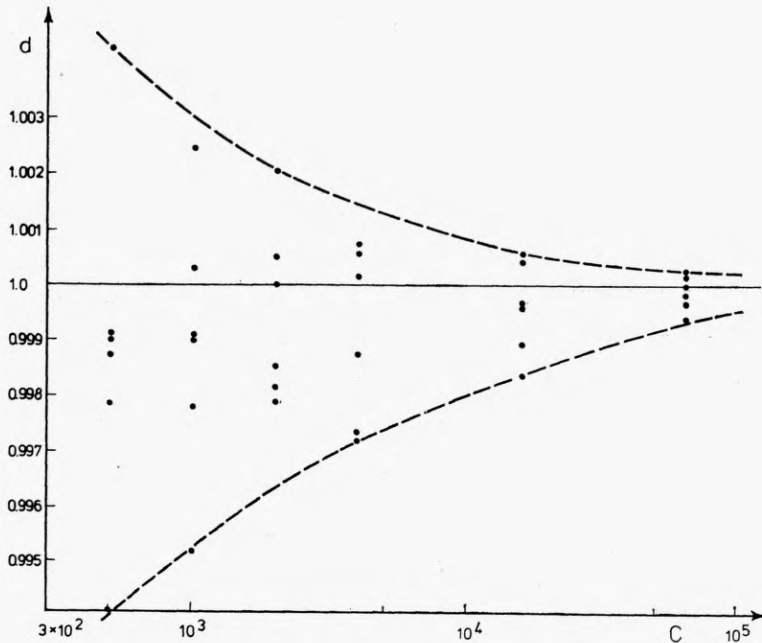
Fig. 4. The dependence of the determined distance d between the maxima on the value of c. The assumed value of d is equal to 1 (for explanation see fig. 3)

of the value c. The results shown in figs. 3 and 4 were obtained for the curve with a relatively "sharp" maximum ($\Gamma_L = 0.03$, $\Gamma_D = 0.18$).

Figures 5 and 6 present analogous dependences for the curve with a "flat" maximum ($\Gamma_L = 0.3$, $\Gamma_D = 0.31$). The systematic deviation of the position of the maximum is connected with the "quasi-quenching", and with an asymmetry caused by the simulation of the second component using eq. (18). Owing to the periodic character of $A(x)$ this systematic deviation does not play any role, since it does not change the distance between the maxima. When the line profile is reduced to the profile of an isolated line the position of the maximum of the curve $B(x)$ is changed. Since the profiles of spectral lines analysed are symmetric, the final position of the maximum is assumed to be the position of the middle of the sector Δx, which joins such points on the distribution $B(x)$ for which the value of the signal is equal to the half of the values at maximum.

Figures 7 and 8 show the dependence of the mean value of the relative errors of the Γ_L and Γ_D:

$$\frac{\delta \Gamma_L}{\Gamma_L} = \left| \frac{\Gamma_{L_{\text{theor}}} - \Gamma_{L_{\text{calc}}}}{\Gamma_{L_{\text{theor}}}} \right| \text{ and } \frac{\delta \Gamma_D}{\Gamma_D} = \left| \frac{\Gamma_{D_{\text{theor}}} - \Gamma_{D_{\text{calc}}}}{\Gamma_{D_{\text{theor}}}} \right|$$

on the value of parameter c for $\Gamma_L = 0.03$, $\Gamma_D = 0.18$. These computations were performed for six different distributions of errors on the
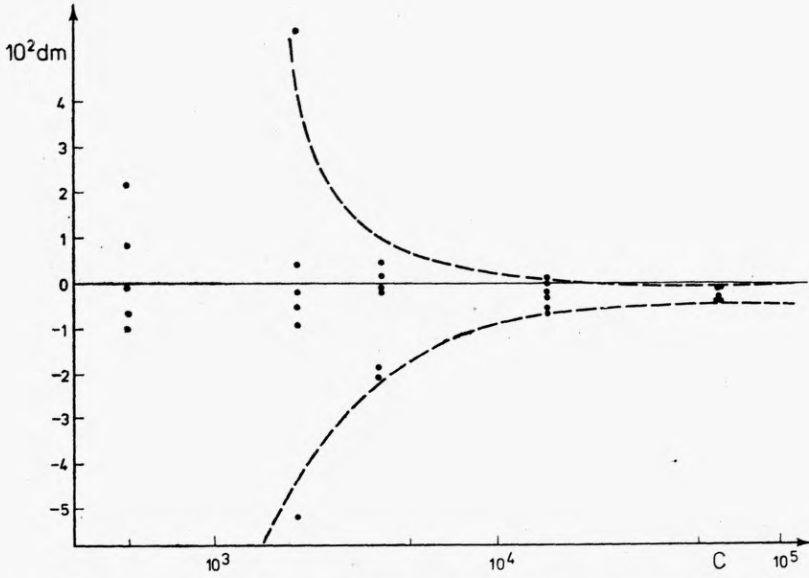
Fig. 5. The deviation *dm* of the determined position of the first interference maximum
as a function of *c*, for $\Gamma_L = 0.3$, $\Gamma_D = 0.3$ (for explanation see fig. 3)
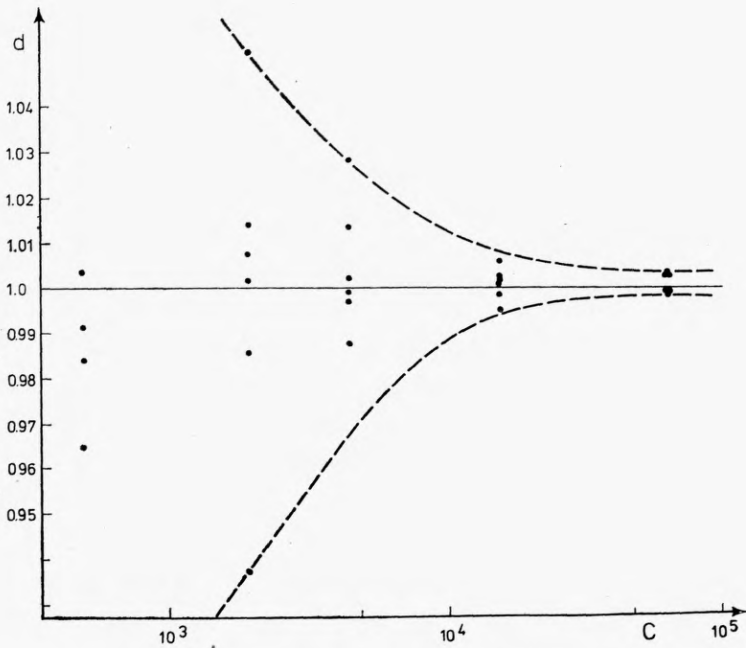
Fig. 6. Dependence of the distance *d* between the maxima on *c* for $\Gamma_L = 0.3$, $\Gamma_D = 0.3$.
The assumed value of *d* is equal to 1 (for explanation see fig. 3)
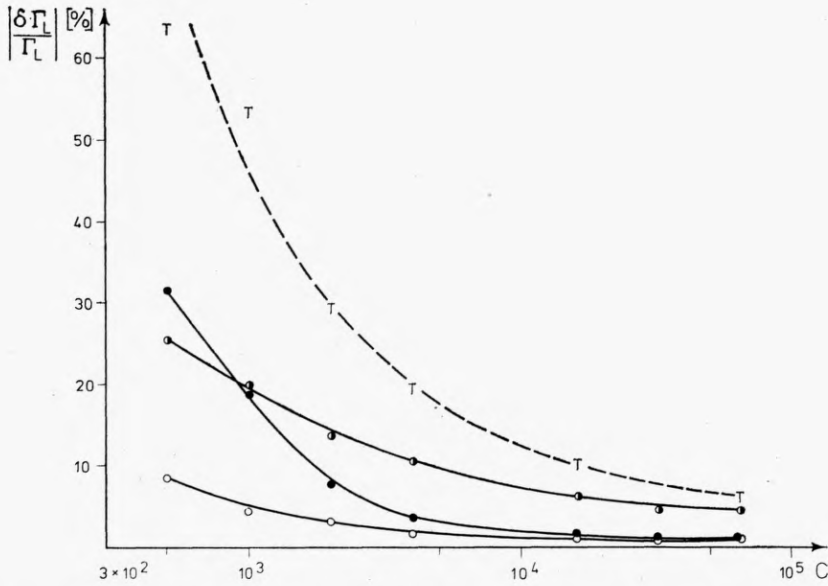
Fig. 7. Dependence of the mean value of the relative error of Γ_L on c. The mean values were calculated as the arithmetic mean of the absolute values of errors obtained for 6 distributions of errors on the curve:

● — the method 1, ◐ — the method 2, ○ — the method 3, T — the largest error occurring for one of the six distributions of errors on the curve obtained within one of the three methods used ($\Gamma_L = 0.03$, $\Gamma_D = 0.2$)
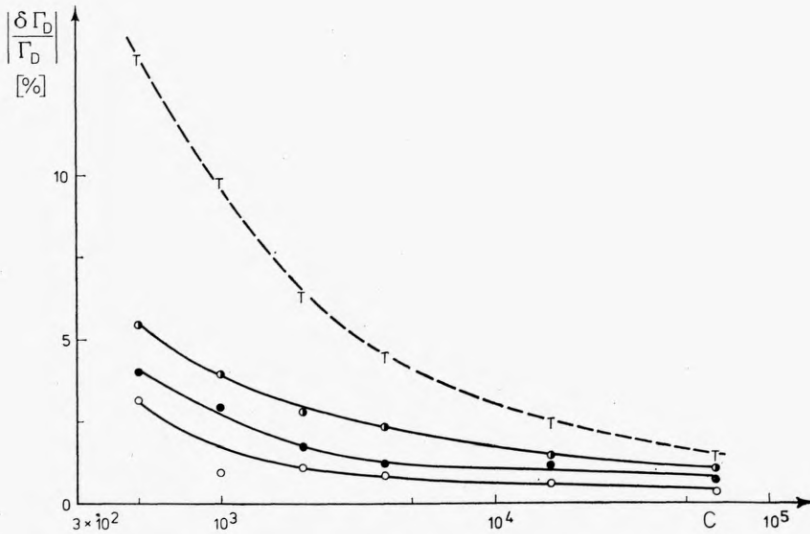
Fig. 8. Dependence of the mean value of the relative error of Γ_D on c (for explanation see fig. 7)

curve. Hence, for every c we have obtained six calculated values of Γ_L and Γ_D for different distribution of errors on the curve. This means that we have obtained six different errors for Γ_L and Γ_D. The error indicated in figs. 7 and 8 has the largest value of all the 18 values of errors determined by using three methods discussed in section ,,Numerical analysis of the Fabry-Pérot interferogram" (6 errors for each method). The mean errors are also shown in figs. 7 and 8. In further analysis only one distribution of errors on the curve was applied, namely that for which the errors of calculated values of Γ_L and Γ_D are close to the mean errors shown in figs. 7 and 8.

Figures 9 and 10 present the dependence of the relative error of the Lorentzian width and the Doppler temperature (for different values of c)
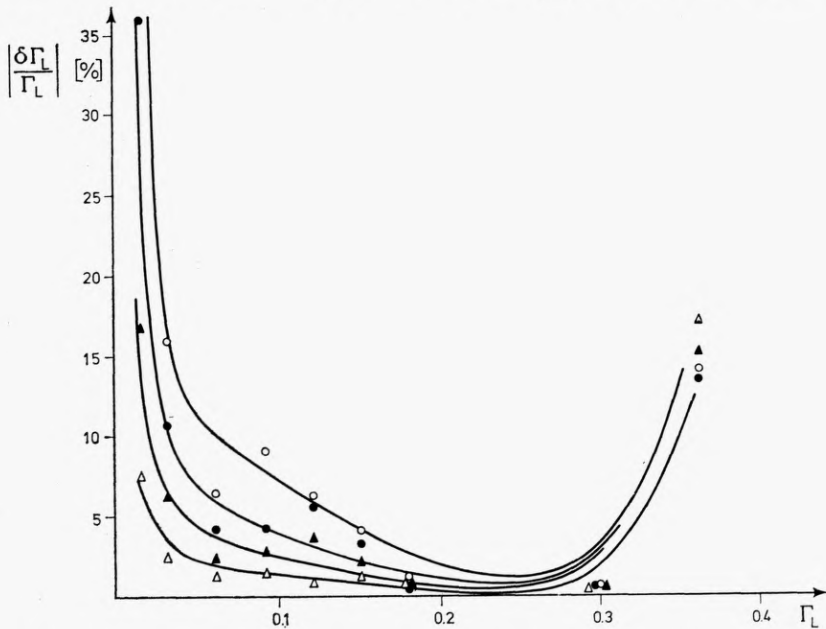
Fig. 9. Dependence of the relative error of Γ_L at $\Gamma_D = 0.18$, for four values of c: $\bigcirc - c = 500$, $\bullet - c = 1000$, $\blacktriangle - c = 2000$, $\triangle - c = 16000$. All calculations were performed for the same distribution of errors on the curve

on the Γ_L, at $\Gamma_D = 0.18$. As it can be seen from figs. 9 and 10, the example analysed in figs. 7 and 8 corresponds to the limiting situation, for which the reliable results may still be obtained. Similar dependence of the errors of the magnitudes Γ_L and Γ_D on the value of Γ_L are shown in figs. 11 and 12 for $\Gamma_D = 0.3$, and for $\Gamma_D = 0.1$ in figs. 13 and 14. The calculations were performed by assuming two values of the photomultiplier background, namely 36 and 100 pulses in the counting time. It turned out that for $c \geqslant 1000$ pulses the results are practically identical for both the values of the background. The data discussed above were obtained for the mean value of the background equal to 36 pulses.
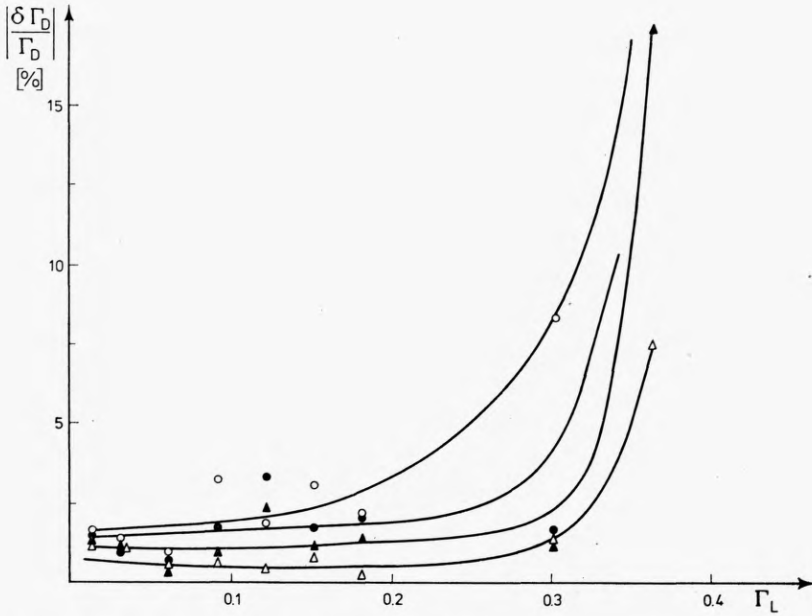
Fig. 10. Dependence of the relative error of Γ_D on Γ_L (for explanation see fig. 9)
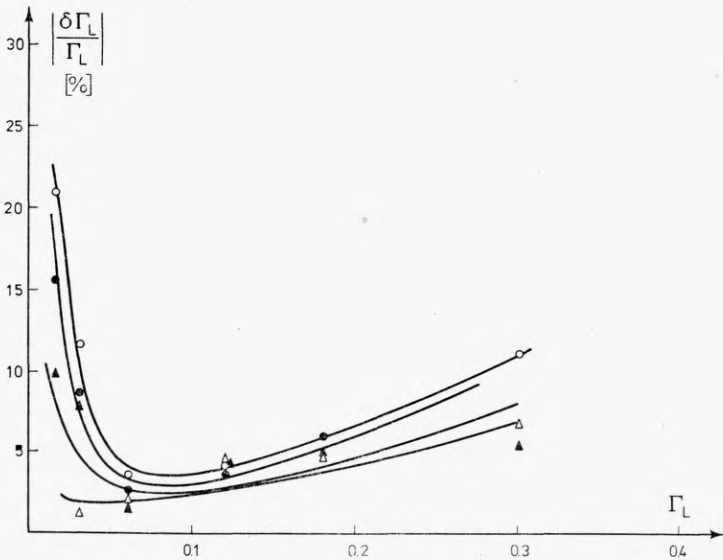
Fig. 11. Relative error of Γ_L vs. Γ_L at $\Gamma_D = 0.3$ (for explanation see fig. 9)

An additional factor which may influence the results of the analysis of the interferograms, particularly for weak lines, is the accuracy of the value of the substracted background of photomultiplier. In order to
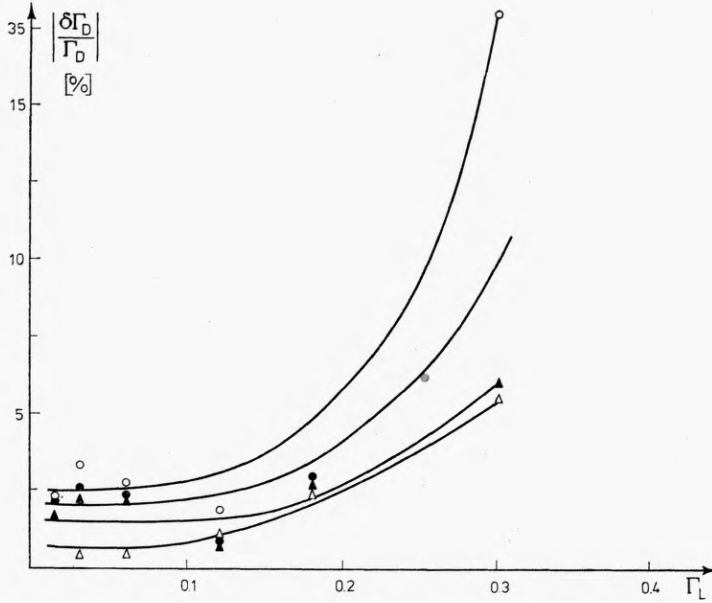
Fig. 12. Relative error of Γ_D, vs. Γ_L at $\Gamma_D = 0.3$ (for explanation see fig. 9)
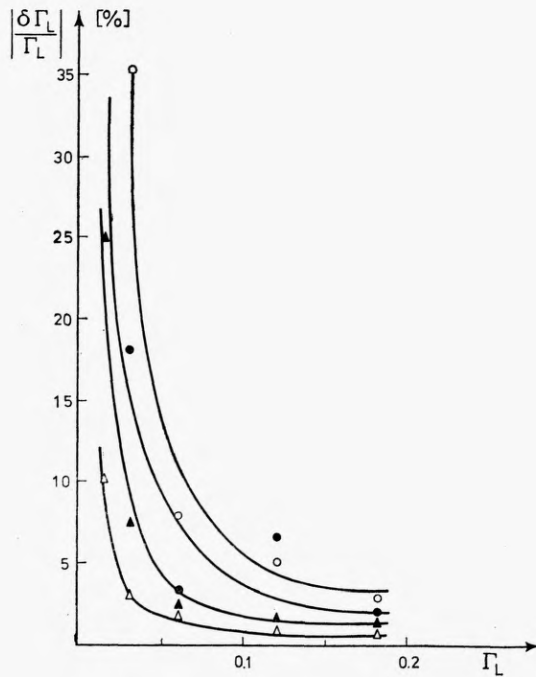
Fig. 13. Relative error of Γ_L vs. Γ_L at $\Gamma_D = 0.1$ (for explanation see fig. 9)
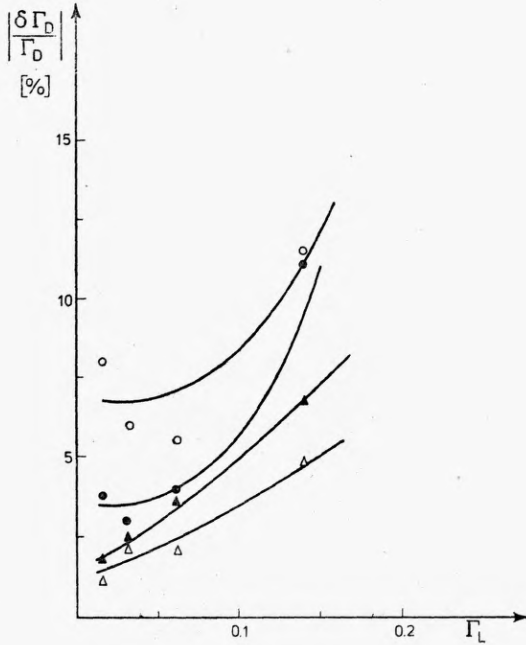
Fig. 14. Relative error of Γ_D on Γ_L at $\Gamma_D = 0.1$ (for explanation see fig. 9)

estimate the influence of the error of the substracted value of the background on Γ_L and Γ_D the following computations have been performed:

For the value of the mean background equal to 36 pulses and for different values of c ($c = 1000, 3000, 6000$) the error has been simulated. From the curves obtained in this way the values of the mean background smaller and greater than the real value 36 have been substracted.

Figure 15 shows the dependence of the results of calculations of Γ_L and Γ_D for $c = 1000$ on the value $\bar{S}$ of the subtracted mean background. The simulation of error has been performed for $\Gamma_L = 0.06$ and $\Gamma_D = 0.18$, and for the value of the mean background equal to 36 pulses. This gives the value of the signal at the maximum together with the real mean background about 200, i.e. $B(0)/B(\pi) = 5$. As it can be seen from fig. 15 one obtains a linear dependence of Γ_L and Γ_D on the value $\bar{S}$ of the subtracted mean background. Similar results were obtained for other values of c. It should be noted that the slopes Z_D and Z_L of the straight lines in fig. 15, representing the respective dependences of Γ_D and Γ_L on $\bar{S}$, depend on the method used in the analysis. The slopes given by the method of BALLIK [6] are about 1.3–1.6 times greater than those given by the methods 2 and 3. Fig. 16 presents the dependence of the slopes Z_D and Z_L on the value of c determined by means of the Ballik method. As it can be seen from fig. 16, for $c \geqslant 5000$ the values of Z_D become practically constant.
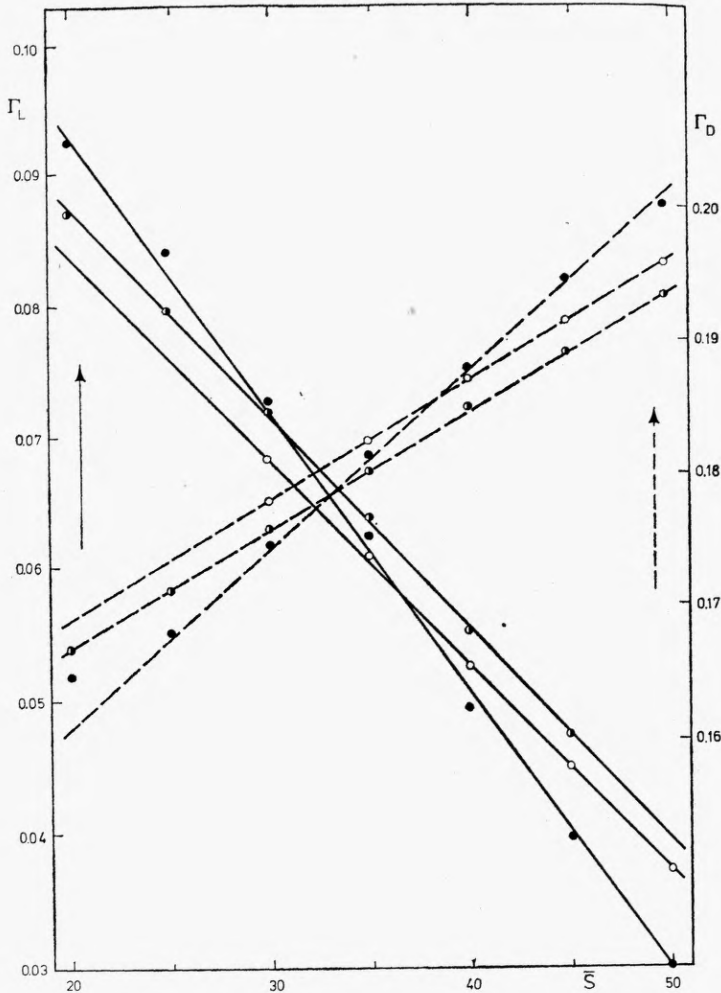
Fig. 15. Dependence of calculated values of Γ_L and Γ_D at $c = 1000$ on the value of the mean background $\bar{S}$. The simulation of error was performed for $\bar{S} = 36$ pulses, $\Gamma_L = 0.06$, $\Gamma_D = 0.2$; ● — method 1, ◑ — method 2, ○ — method 3

Summarizing remarks

A procedure of the curve "composing" has an essential influence on the further analysis of the interferograms. The value of the calculated distance between the maxima, which can be compared with the value characteristic for the particular experimental apparatus is the measure of the accuracy of the "composing" procedure. In the apparatus described in [4] this characteristic value is equal to the ratio of the length of the Jamin interferometer to the distance between the plates in the FPI. As it can be seen from fig. 4 the discrepancies of the results calculated for narrow
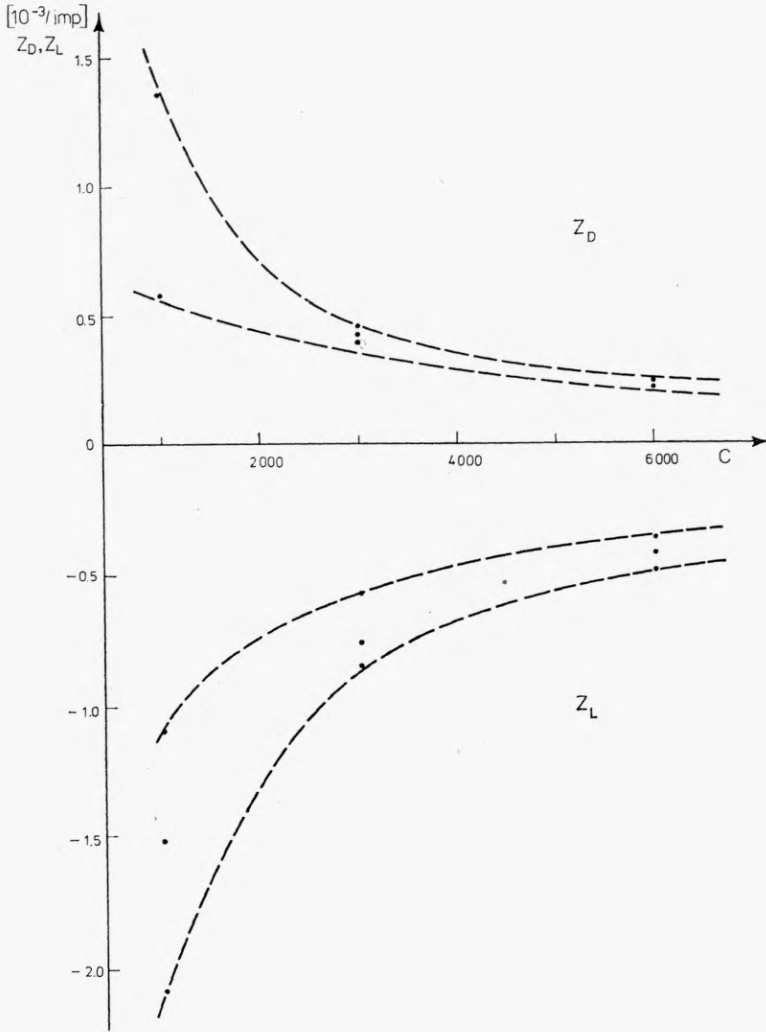
Fig. 16. Dependence of the slope for the method 1 as a function of c. For each c the simulation of errors was carried out for three values of the signal at the minimum by changing the values of Γ_L (the value of the signal with background s was then changed from 70 to 200)

lines ($\Gamma_L = 0.03$, $\Gamma_D = 0.18$) are within the 1/68 part of the free spectral region as early as for $c = 500$ pulses. For lines with flat maxima ($\Gamma_L = 0.3$, $\Gamma_D = 0.31$) similar discrepancies are found only for $c \geqslant 10000$ (see fig. 6). The analysis of figs. 4 and 6 enables to reject the results of measurements charged with large errors, in particular those caused by large noise in the vicinity of the maximum. As it can be seen from figs. 9–14, for $c > 1000$ pulses we can determine these values Γ_L which are charged only by a little error. Namely, from the comparison of dependences shown in

figs. 9–14, corresponding to these values of $\Gamma_D(0.1, 0.2, 0.3)$ it can be concluded that the change of the Doppler width in this region affects essentially these values of Γ_L, which are not charged with a large error. For instance, if $0.03 < \Gamma_L < 0.3$ then for $c > 1000$ the relative errors of both the computed Lorentz width and the Doppler temperature do not exceed $10^0/_0$.

Figure 15 shows that the Ballik method (method 1), being a very accurate one, is simultaneously the most sensitive to the background error. As it follows from the dependence shown in fig. 16, the influence of the background error on the values of Γ_L and Γ_D, determined by the method 1, is small for $c > 5000$. For the methods 2 and 3 the situation is more profitable.

In the conclusion we can say that, if the accurate value of the mean background is known, then for the "narrow" lines ($\Gamma_L \approx 0.03$, $\Gamma_D \approx 0.2$) the lower limit of the measured signal at the line maximum cannot be lower than 1000 pulses and for the "broad" lines ($\Gamma_L \approx 0.3$, $\Gamma_D \approx 0.3$) it cannot be lower that 5000 pulses. When the value of the mean background is known with a low accuracy then both for the "narrow" and "broad" lines c should be greater than 5000. Results obtained in experiment are in full accordance with the above conclusions.

Appendix

Tables of function $\varepsilon(h)$ and $Y(h)$

Table of function $\varepsilon(h)$

h	0	1	2	3	4	5	6	7	8	9
0.0	0.6366	0.6366	0.6367	0.6368	0.6370	0.6373	0.6376	0.6379	0.6383	0.6388
0.1	0.6394	0.6400	0.6408	0.6416	0.6425	0.6434	0.6445	0.6457	0.6469	0.6482
0.2	0.6497	0.6512	0.6529	0.6546	0.6565	0.6584	0.6604	0.6626	0.6648	0.6672
0.3	0.6696	0.6722	0.6748	0.6775	0.6804	0.6833	0.6863	0.6893	0.6925	0.6957
0.4	0.6990	0.7024	0.7059	0.7094	0.7129	0.7166	0.7203	0.7240	0.7278	0.7316
0.5	0.7355	0.7394	0.7433	0.7473	0.7513	0.7553	0.7594	0.7635	0.7676	0.7717
0.6	0.7758	0.7800	0.7842	0.7883	0.7925	0.7967	0.8009	0.8051	0.8093	0.8135
0.7	0.8177	0.8219	0.8262	0.8304	0.8345	0.8387	0.8429	0.8471	0.8513	0.8554
0.8	0.8596	0.8637	0.8678	0.8719	0.8760	0.8801	0.8842	0.8882	0.8923	0.8963
0.9	0.9003	0.9043	0.9083	0.9122	0.9162	0.9201	0.9240	0.9279	0.9318	0.9356
1.0	0.9394									

Table of function $Y(h)$

h	0	1	2	3	4	5	6	7	8	9
0.0	1.0000	0.9901	0.9804	0.9710	0.9618	0.9528	0.9441	0.9357	0.9275	0.9195
0.1	0.9118	0.9044	0.8973	0.8905	0.8839	0.8776	0.8716	0.8659	0.8605	0.8553
0.2	0.8505	0.8459	0.8416	0.8376	0.8339	0.8305	0.8273	0.8244	0.8217	0.8194
0.3	0.8172	0.8154	0.8137	0.8123	0.8112	0.8102	0.8095	0.8090	0.8087	0.8086
0.4	0.8087	0.8089	0.8094	0.8100	0.8108	0.8118	0.8129	0.8142	0.8156	0.8171
0.5	0.8188	0.8206	0.8225	0.8246	0.8268	0.8290	0.8314	0.8339	0.8365	0.8392
0.6	0.8420	0.8448	0.8478	0.8508	0.8539	0.8571	0.8603	0.8636	0.8670	0.8705
0.7	0.8740	0.8776	0.8812	0.8849	0.8886	0.8924	0.8963	0.9001	0.9041	0.9081
0.8	0.9121	0.9162	0.9203	0.9244	0.9286	0.9329	0.9371	0.9414	0.9457	0.9501
0.9	0.9545	0.9589	0.9634	0.9679	0.9724	0.9769	0.9815	0.9861	0.9907	0.9953
1.0	1.0000									

References

[1] MATYUGIN Yu. A., PROVOROV A. C., TSCHEBOTAYEV V. P., Zhurn. Exper. Theor. Phys. **63** (1972), 2043.

[2] WOLNIKOWSKI J., Bull. Acad. Polon. Sci., Ser. sci. math. astronom. et phys. **24** (1976), 815.

[3] KRYLOVA S. I., LUISOVA L. A., KHAKHAEV A. D., Zhurn. Prikl. Spektr. **14** (1971), 919.

[4] BIELSKI A., KANDELA S. A., WOLNIKOWSKI J., TURŁO Z., Acta Phys. Polon. **A42** (1972), 295.

[5] RAUTIAN S. G., Uspiekhi Fiz. Nauk **66** (1958), 475.

[6] BALLIK E. A., App. Opt. **5** (1966), 170.

[7] KUHN H. G., VAUGHAN J. M., Proc. Roy. Soc. **A277** (1963), 297.

[8] BIELSKI A., KARWOWSKI J., WOLNIKOWSKI J., Opt. Comm. **23** (1977), 362.

[9] *Theory of Measurements*, ed. Szydłowski, PWN, Warszawa 1974 (in Polish).

[10] ZIELIŃSKI R., *Random Numbers Generators*, WNT, Warszawa 1972 (in Polish).

[11] MITCHEL A. C. G., ZEMANSKY M. W., *Resonance Radiation and Excited Atoms*, University Press, Cambridge 1961.

О численном анализе интерферограмм Фабри–Перо

Обсуждается и испытывается три метода численного определения параметров профила Фоигта по интерферограммам Фабри–Перо. Произведено симуляцю ошибки в предположении что она обусловлена конечным числом фотонов в сигнале. Оценивается наименьшая величина интенсивности света в максимуме спектральной линии и область лоренцовской и гауссовской полуширины при которых получается достоверные результаты.